

Increasing SAM Zero-Shot Performance on Multimodal Medical Images Using GPT-4 Generated Descriptive Prompts Without Human Annotation

Zekun Jiang[#], Dongjie Cheng[#], Ziyuan Qin, Jun Gao, Qicheng Lao, Kang Li*, Le Zhang*

Abstract: This study develops and evaluates a novel multimodal medical image zero-shot segmentation algorithm named Text-Visual-Prompt SAM (TV-SAM) without any manual annotations. TV-SAM incorporates and integrates large language model GPT-4, Vision Language Model GLIP, and Segment Anything Model (SAM), to autonomously generate descriptive text prompts and visual bounding box prompts from medical images, thereby enhancing SAM for zero-shot segmentation. Comprehensive evaluations are implemented on seven public datasets encompassing eight imaging modalities to demonstrate that TV-SAM can effectively segment unseen targets across various modalities without additional training, significantly outperforming SAM AUTO and GSAM, closely matching the performance of SAM BBOX with gold standard bounding box prompts, and surpassing the state-of-the-art on specific datasets like ISIC and WBC. The study indicates that TV-SAM serves as an effective multimodal medical image zero-shot segmentation algorithm, highlighting the significant contribution of GPT-4 to zero-shot segmentation. By integrating foundational models such as GPT-4, GLIP, and SAM, it could enhance the capability to address complex problems in specialized domains. The code is available at: <https://github.com/JZK00/TV-SAM>.

Key words: large language model; vision language model; segment anything model; medical image segmentation; zero-shot segmentation; GPT-4.

1 Introduction

As the first vision foundation model, Segment Anything Model (SAM)' emergence has spurred researchers worldwide to explore its zero-shot segmentation performance in various scenarios [1-3], especially in the field of medical imaging [4-13]. In

- Zekun Jiang, Jun Gao, and Le Zhang are with the College of Computer Science, Sichuan University, Chengdu, Sichuan, China. E-mail: jiangzekun@stu.scu.edu.cn; gaojun@stu.scu.edu.cn; zhangle06@scu.edu.cn.
- Dongjie Cheng and Kang Li are with the West China Biomedical Big Data Center, West China Hospital, Sichuan University, Chengdu, China. E-mail: chengdongjie@stu.scu.edu.cn; likang@wchscu.cn.
- Ziyuan Qin is with Case Western Reserve University, Cleveland, US. E-mail: ziyuan.qin@case.edu.
- Qicheng Lao is with School of Artificial Intelligence, Beijing University of Posts and Telecommunications, Beijing, China. E-mail: qicheng.lao@bupt.edu.cn.

The authors contributed equally to this work.

* To whom correspondence should be addressed.

Manuscript received: year-month-day; accepted: year-month-day.

clinical practice, medical images are the primary basis for decision-making in disease diagnosis and treatment. Since medical imaging typically consists of multiple modalities with different organs of the human body, it usually makes segmentation scenarios very complex [14]. Therefore, if we can find an effective zero-shot segmentation method which can eliminate the need to train related segmentation models by supervised, weakly supervised, or transfer learning, it could greatly help us save the considerable data and computational resources.

Currently, SAM has three prompt working modes, which are no-prompts, point prompts, and box prompts [7], but it cannot directly use text prompts for auto segmentation. The open-source community has provided several alternative solutions, such as GroundedSAM [15], but they still rely on human annotations as prompt inputs. Thus, we consider that they are insufficient for automatic medical image segmentation. Furthermore, the current evaluation

studies of SAM's zero-shot segmentation mostly rely on points or boxes generated from ground truth masks as prompt inputs [6, 8]. Undoubtedly, they are not applicable for the dataset or domain lacking annotated information, and thus cannot be directly generalized for use for clinical applications.

Therefore, exploring a zero-shot segmentation algorithm for multimodal medical images is a highly worthwhile endeavour. In previous studies, Qing et al. [16] proposed the use of a Vision Language Model (VLM) to obtain bounding boxes (bboxes), which could facilitate segmentation. Since it is not only challenging to accurately provide text prompts for VLM, but also experimental results indicate that the representations learned by existing VLMs still exhibit a significant domain gap with medical data [16], relying solely on VLMs fails to yield sufficiently high-quality results.

Recently, Large Language Model (LLM), with their unique capabilities such as emergence and chain of thought [17, 18], have brought the concept of foundation model into the public eye. Particularly, GPT-4 has essentially become the most powerful intelligence model to date [19]. Thus, it could be a completely viable approach for us to employ GPT-4 as a knowledge source to design a better expressive prompt for medical concepts.

For these reasons, this study developed a novel zero-shot segmentation algorithm by integration of GPT-4 prompts, VLM, and SAM. And we extensively evaluated the approach on multimodal medical image datasets, comparing it with other zero-shot segmentation methods to demonstrate its superiority.

1.1 Related work

VLM: Zero-shot segmentation enables models to recognize and segment objects in downstream tasks that have not been seen before without additional training. A groundbreaking work about zero-shot learning in computer vision is CLIP [20]. As a VLM, CLIP leverages contrastive learning on images and text to generate a shared multimodal representation. Based on this multimodal representation, semantic segmentation on unseen images can be achieved. Consequently, CLIP and its subsequent extensions

have been applied to medical image segmentation tasks. Liu et al. [21] has built a CLIP-driven universal model for organ segmentation and tumor detection. Qin et al. [16] also demonstrated that rapid adaptation to unknown medical image data for target detection can be achieved through the integration of prompts and GLIP [22].

Though preliminary exploratory efforts already made great progress, how to optimize the prompts given to VLMs and automatically extract expressive high-quality prompts from medical images is still an important topic that needs further exploration.

SAM: With the emergence and development of SAM, zero-shot learning has become increasingly popular. Generalist foundation models learned more diverse and extensive multimodal representations and possess unprecedented capabilities. Over the past few months since the publication of SAM, research teams from around the world have extensively assessed SAM's segmentation performance in diverse medical imaging scenarios from various perspectives. Several previous studies collected dozens of medical image datasets to assess SAM's segmentation performance [6, 8], but no particularly intriguing conclusions were drawn. In a nutshell, SAM without any prompts often exhibits poor segmentation performance, while it shows very stable performance with multiple points or bbox prompts. This problem could be caused by the huge domain gap between medical images and the nature images.

For this reason, the further studies have fine-tuned SAM and developed specialized models for medical image processing, such as MedSAM [5], SAM-Med2D/3D [23, 24], etc.

On the one hand, these methods all require point or bbox as visual prompts and visual prompts need manual input, failing to achieve satisfactory segmentation in zero-shot settings without any prompts. Additionally, works like SAM-Med2D/3D requests substantial data and computational resources investment during the fine-tuning process [23, 24]. Therefore, the exploration of SAM application is still ongoing.

On the other hands, this leads to a debate

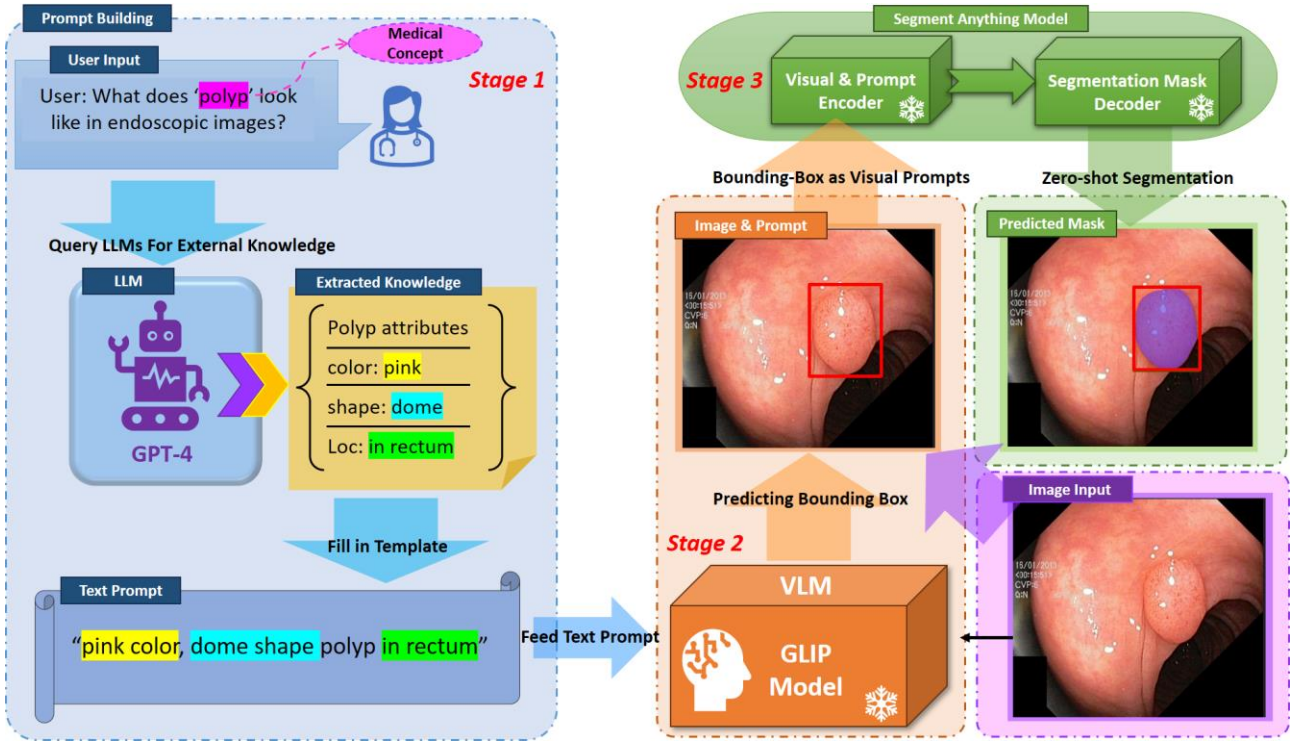


Fig. 1 Proposed Zero-shot Algorithm Framework for Medical Image Segmentation

regarding generalist and specialist models. We often argued that for medical imaging, specialist models, once fine-tuned, may prove more effective. However, previous studies [25] turn out that generalist models still possess untapped potential with ingenious prompt engineering. Even for the concepts not present in their pre-training, these models can be effectively 'activated' by prompts that employ analogical understanding of the concepts along with detailed descriptions of the visual nuances [25, 26]. Consequently, we can achieve performances unattainable by a single generalist model alone by blending various generalist models.

GPT-4: It has been explored for medical image processing [19, 27]. However, using GPT-4 directly for image processing encounters various challenges. The main reason is that when facing medical tasks, GPT-4 becomes particularly cautious. It acknowledged that GPT-4 is not a medical professional (e.g., radiologist or pathologist), making it unable to provide more precise answers [27]. In several cases, it may even refuse to recognize certain medical images. Therefore, though the current version of GPT-4 is not recommended for direct use in real-world clinical diagnosis [27], GPT-4 can be indirectly

employed by generating rich descriptive prompts, thereby activating and enhancing the recognition and segmentation performance of VLM and SAM.

In summary, VLMs, SAM, or GPT-4 have shown promising potential in zero-shot segmentation, but are still not perfect. Currently, there is no research exploring the effective integration of these methods to achieve better segmentation results.

1.2 Key contributions

Therefore, this study introduced a novel zero-shot segmentation algorithm for medical images, named Text-Visual-Prompt SAM (TV-SAM), which was co-driven by GPT-4 prompts, VLM (GLIP), and SAM. TV-SAM contributes the following:

1. We proposed a GPT-4 driven SAM zero-shot segmentation algorithm for medical images and carried out comprehensive evaluations for multimodal medical image datasets with eight modalities and nine targets.
2. We developed a novel zero-shot segmentation algorithm framework for medical images. By integrating LLM and VLM into SAM, we not only automatically generate text prompts and visual prompts based on input images, but also segment the objects without any additional human prompt.

3. Our approach demonstrates better segmentation performance than SAM without prompts and GSAM. In several scenarios, the performance approximates the SAM with gold standard bbox prompts. The experimental results indicated while this method can function as a zero-shot segmentation tool, the overall segmentation performance still needs improvement, particularly for radiology images.

2 Methodology

Before delving into the specifics, we first provide an overview of our workflow from a high-level perspective by Fig. 1. In general, our methodology TV-SAM consists of three primary stages: first is the generation of text prompts; second is the creation of visual prompts; third is the mask decoding stage.

In the first stage, we employ GPT-4 as knowledge sources to generate text prompts that vividly describe medical concepts with expressive detail of medical images.

Transitioning to the second stage, we employ pre-trained VLMs to identify the probable regions of the medical concepts based on the provided prompts, typically using a bounding box format.

In the third stage, the bounding boxes for the areas of interest are employed as visual prompts to assist the SAM in more accurately predicting the segmentation masks for these areas.

In summary, users only supply unlabeled medical images along with the concepts, objects, or abnormalities of interest. Subsequently, TV-SAM autonomously executes the three stages and generates the corresponding segmentation masks.

2.1 GPT-4 as knowledge sources for expressive prompts design

To generate the text prompts, we present the GPT-4 driven expressive prompts design algorithm as stage 1 of Fig. 1. Here, we employ GPT-4 as an external knowledge source to generate detailed text prompts for medical concepts in medical images.

$$F_I = \text{ImageEncoder}(I) \quad (1)$$

$$F_P = \text{PromptEncoder}(P) \quad (2)$$

$$F_{fusion} = \text{CrossAttention}(F_I, F_P) \quad (3)$$

Specifically, we feed images I and a dialogue template as P into GPT-4 model. GPT-4 employs a separate vision encoder to extract high-level features F_I from the image I by Eq. (1) and uses a text encoder to get F_P from P by Eq. (2). Through cross-attention, the representations from both are fused to have F_{fusion} and embedded into the LLM by Eq. (3).

$$D_{LLM} = \text{Decoder}(F_{fusion}) \quad (4)$$

Then, with a decoder to return the specific information D_{LLM} about the target concept by Eq. (4), including attributes such as color, shape, and location.

Upon acquiring these attributes, we employ an additional template, Temp_prompt, to construct the final text prompts by incorporating the obtained attributes. This process can be executed independently or directly embedded into the dialogue template, guaranteeing that the information returned by GPT conforms to the final prompt format.

2.2 Generating visual prompts via VLM

As previously articulated, the application of the SAM in medical imaging predominantly relies on human-labeled visual prompts, such as bounding boxes or center points. While we acknowledge that providing visual prompts demands less effort compared to creating ground truth segmentation masks, the curation of visual prompts for all samples remains a non-trivial task. This is primarily due to the requirement of expert-level knowledge to identify areas of interest accurately. For these reasons, we employ VLMs to generate visual prompts automatically as stage 2 of Fig. 1.

Here, we selected GLIP [22] as the foundational VLM, the input image I is fed back into GLIP image encoder to obtain F_I as shown in Eq. (1), and the previously obtained descriptive prompts D_{LLM} serve

as text prompts P into GLIP prompt encoder to have F_p by Eq. (2). This essentially achieves zero-shot object detection.

$$B_{VLM} = \text{BboxDecoder}(F_{fusion}) \quad (5)$$

Then, the F_{fusion} is generated by Eq. (3) and embedded into a bbox decoder to predict bounding boxes B_{VLM} by Eq. (5).

It is important to note that the quantity of predicted bounding boxes typically exceeds necessity and thus requires reduction via the Non-Maximum Suppression algorithm [28]. Moreover, we further refine the selection by filtering out any predicted boxes that exhibit a confidence score below a predetermined threshold.

2.3 SAM zero-shot segmentation with visual prompts

The SAM can accept three types of prompts: point, box, and text, but it should be noted that the text prompt variant is not yet publicly available. Since previous research [8] has indicated that the box prompt is particularly effective when applying SAM in the medical domain and the box mode of SAM achieves optimal performance across a range of medical image datasets for our studies [7]. Therefore, we implement a box prompts-based SAM zero-shot segmentation algorithm as stage 3 of Fig. 1.

$$M_{SAM} = \text{MaskDecoder}(F_{fusion}) \quad (6)$$

As shown in Eq. (1-3), we re-input the image I into SAM image encoder to obtain F_I , and input the

bounding boxes B_{VLM} predicted by GLIP as visual prompts P into SAM prompt encoder to obtain F_p .

Then, the F_{fusion} is input into the SAM mask decoder to generate accurate segmentation masks M_{SAM} by Eq. (6).

3 Experiment

3.1 Datasets

For a comprehensive evaluation of the efficacy of our approach in clinical practice, we collected seven publicly available datasets as the multimodal medical imaging datasets, encompassing eight distinct medical imaging modalities and nine segmentation objects. Table 1 lists the general distribution of the datasets. Because our algorithm does not need any training, here we directly used the test set of the public datasets as the evaluation data. Detailed descriptions of the datasets are provided as follows:

(1) Polyp benchmark: The diagnosis of gastrointestinal diseases often involves endoscopic imaging. This dataset consists of endoscopic images specifically focusing on polyps and associated neoplastic changes in the colon and rectum, with corresponding masks delineating the polyps.

(2) ISIC 2018: Skin diseases are typically preliminarily diagnosed through regular photographic images. This dataset comprises a substantial number of skin disease images, involving conditions such as melanoma and basal cell carcinoma, with segmented masks for each lesion.

(3) WBC dataset: The diagnosis of blood disorders requires microscopic imaging of blood cells. This dataset comprises hundreds of images of blood cell morphology along with corresponding masks delineating the cell nuclei.

(4) BUSI dataset: Ultrasound scanning is a commonly used diagnostic tool for breast diseases. This dataset comprises ultrasound images of 600 female patients in ages between 25 and 75, with segmentation masks delineating tumor regions.

(5) TN3K dataset: The diagnosis of thyroid diseases primarily relies on ultrasound examinations. This dataset comprises over three thousand thyroid ultrasound images, with masks delineating thyroid nodules.

(6) COVID-19 Database: The diagnosis of lung diseases is inseparable from X-rays and chest CT scans, and this is precisely a database related to COVID-19 chest X-ray images and lung masks.

Table 1. Overall distribution of the datasets.

Dataset	Modality	Segmentation object	Num. evaluated data
Polyp benchmark [29]	Endoscope	Polyp	602
ISIC 2018 [30, 31]	Dermoscopy	Melanoma	1002
WBC [32]	Microscopy	Cell	300
BUSI [33]	Ultrasound	Breast cancer	1312
TN3K [34]	Ultrasound	Thyroid nodules	614
COVID-19 Database [35, 36]	X-ray	Lung	10192
CHAOS [37]	CT, T1 MRI, T2 MRI	Liver, Spleen, Kidney	300, 319, 302

(7) CHAOS dataset: The diagnosis of thoracic and abdominal diseases typically involves radiological imaging, primarily CT and MRI. This dataset combined CT-MRI healthy abdominal organ segmentation, including CT data with liver masks, as well as T1 and T2 MRI data with segmentation masks for the liver, spleen, and kidneys.

3.2 Comparative experiment

To demonstrate the superiority of TV-SAM, we carried out comparative evaluations with various SAM benchmark algorithms, including SAM with no-prompt (SAM AUTO), SAM with gold standard bbox prompts (SAM BBOX), and only using GLIP and SAM (GSAM).

SAM AUTO: This is also called SAM 'everything mode', where images are input into SAM without any prompts, and then SAM generates segmentation masks for targets in the image directly based on the image decoder. However, because there are no prompts for specify targets, the performance of this method is usually not very well, although it can demonstrate better segmentation performance in image scenes with a single clear target.

SAM BBOX: This is implemented based on SAM 'bbox mode'. Among the three modes of SAM, the 'bbox mode' is known to have the best performance. Therefore, the gold standard boxes from the public datasets are used as input prompts, which are input into SAM along with the images. Through prompt encoder, image encoder, and mask decoder, we can obtain accurate segmentation.

GSAM: To demonstrate the contribution of LLM for our study, we also implemented the GSAM algorithm. This algorithm uses only GLIP and SAM to

do segmentation, directly inputting the image and the name of the object to be segmented into GLIP. GLIP identifies targets in the image based solely on the prompts of the object name and returns bbox prompts to SAM for further segmentation.

3.3 Statistical analysis

Segmentation results are evaluated by Dice coefficient, see Eq. (7).

$$Dice(M, M^*) = \frac{2|M \cap M^*|}{|M| + |M^*|} \quad (7)$$

Here, M represents the actual segmentation mask, while M^* represents the predicted segmentation mask. The related distributions are represented by mean values and 95% CIs. Statistical tests between different segmentation performances employ the t-test [38-43], with $P < 0.05$ indicating a significant difference.

4 Results and Discussion

This section presents the results from three key aspects: (1) the quantitative evaluation of our algorithm (TV-SAM) in multimodal medical imaging datasets, (2) the comparison of TV-SAM with other three commonly used SAM-based zero-shot algorithms and supervised learning algorithm, and (3) the comparison of segmentation performance under different bounding box selection strategies.

For the first aspect, Fig. 2 quantitatively assesses the segmentation performance of TV-SAM for each imaging modality dataset.

For non-radiology images, our method achieves an average Dice above 0.8, with the Dice scores on

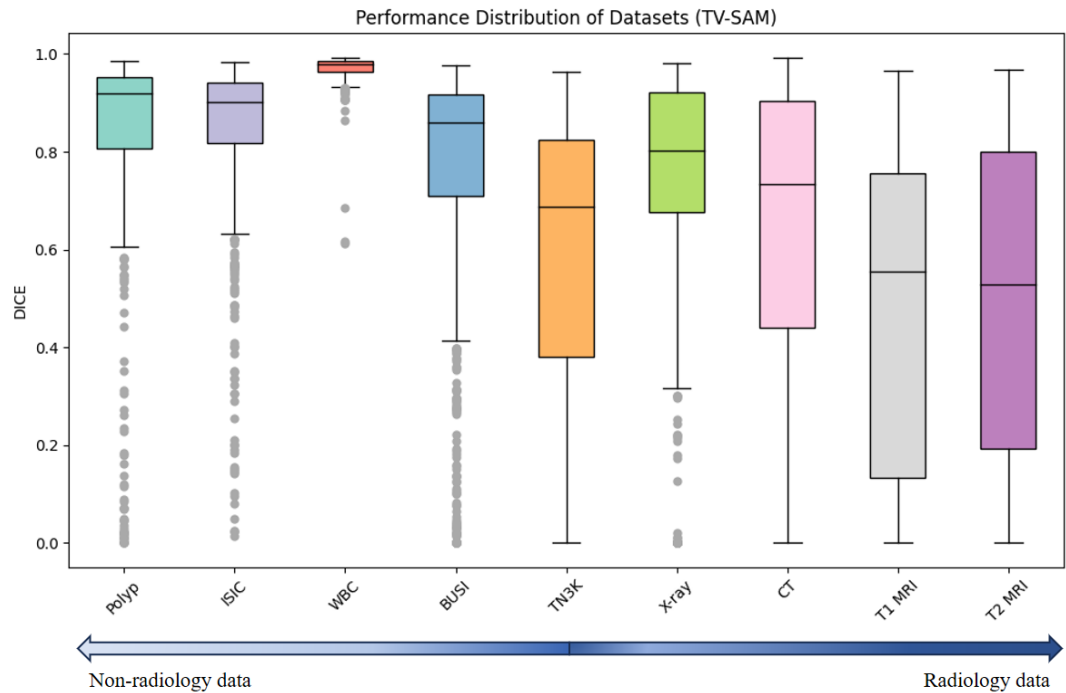


Fig. 2 Performance distribution of TV-SAM in multimodal datasets

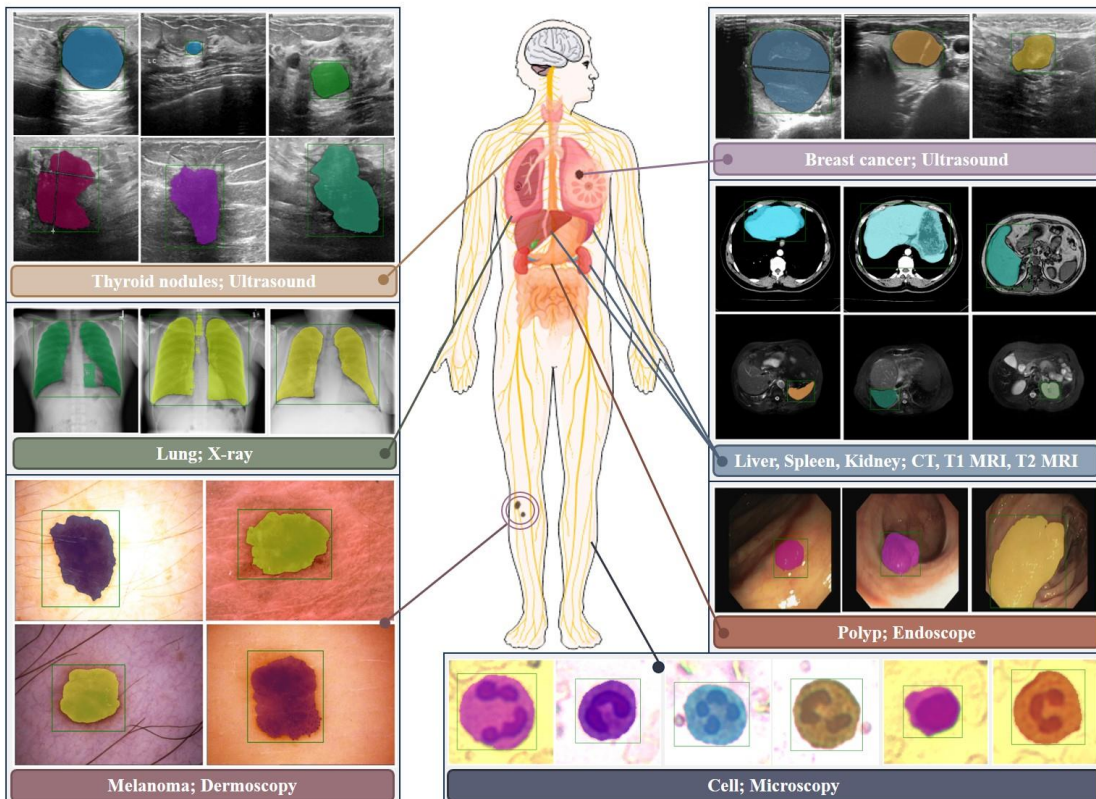


Fig. 3 Overview of Our Zero-shot Segmentation Performance Across Multiple Organs in Multimodal Medical Imaging

Polyp, ISIC, and WBC dataset being 0.831, 0.853, and 0.968, respectively.

However, for radiology images, the segmentation performance is decreased. For BUSI and COVID-19

Table 2. Zero-shot segmentation performance comparison. The value is the average Dice, with bold indicating the best performance.

Methods	Polyp	ISIC	WBC	BUSI	TN3K	X-ray	CT	T1 MRI	T2 MRI
SAM BBOX	0.909	0.8833	0.97	0.8421	0.78	0.7813	0.829	0.5539	0.605
TV-SAM	0.831	0.853	0.968	0.751	0.588	0.788	0.636	0.47	0.488
GSAM	0.453	0.777	0.965	0.734	0.412	0.6297	0.591	0.47	0.441
SAM AUTO	0.654	0	0.955	0.5312	0.4324	0.565	0.63	0.4323	0.406

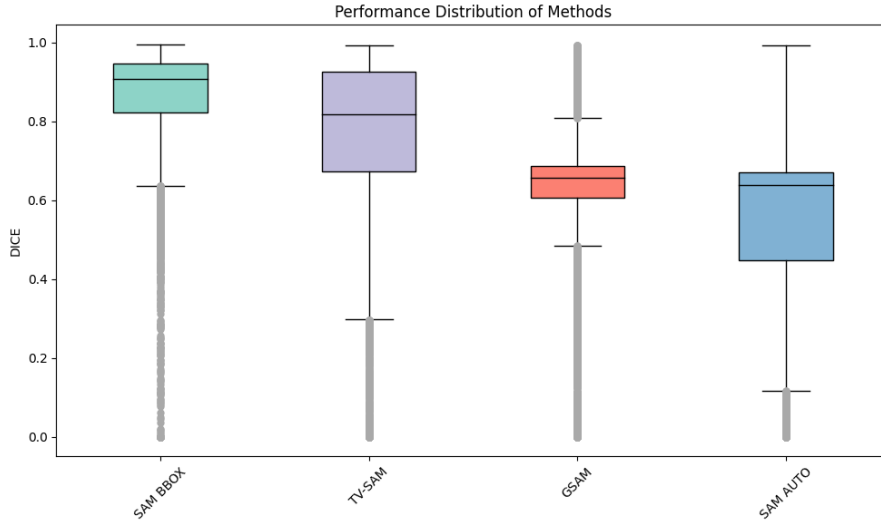


Fig. 4 Performance distribution of different zero-shot segmentation methods

X-ray dataset, the Dice scores are close to 0.8, being 0.751 and 0.788 respectively, while on other datasets such as CT and MRI, the metrics are less than 0.7.

Moreover, Fig. 3 overviews several accurately predicted zero-shot segmentation cases, which help us observe the segmentation results of TV-SAM more visually on cross-organ and cross-modal medical imaging data. It is important to highlight that TV-SAM can directly segment unseen multimodal medical image targets without an additional training process, which provides a new strategy and evidence to solve the complex issues with limited samples and multimodality in the medical imaging field.

In other words, fully leveraging the general knowledge representations of foundational models by GPT-4 and SAM, along with appropriate prompt techniques for knowledge activation, can be directly applied to address complex problems in specialized domains.

For the second aspect, Table 2 provides a performance comparison of TV-SAM with SAM

AUTO, SAM BBOX, and GSAM across different datasets, which demonstrates the advantages of TV-SAM as a novel zero-shot segmentation algorithm. Additionally, Fig. 4 shows a comparison of the segmentation performance distribution of these methods across the entire multimodal medical imaging dataset.

Table 3. TV-SAM versus SOTA on non-radiology datasets. The value is the average Dice and the bold indicates the best performance.

Methods	Polyp	ISIC	WBC
TV-SAM	0.831	0.853	0.968
SOTA	0.898	0.802	0.883

Table 2 and Fig. 4 turn out that, on the one hand, different zero-shot methods generally exhibit the same pattern across various modality datasets, that is, greater average segmentation performance on non-radiology images, and less performance on radiology images such as CT and MRI; On the other hand, TV-SAM is better than SAM AUTO ($P < 0.01$) and GSAM

Table 4. Performance comparison under different bounding box selection settings. The values represent the average Dice and the bold indicates the best performance.

Methods	Polyp	ISIC	WBC	BUSI	TN3K	X-ray	CT	T1 MRI	T2 MRI
TOP-1	0.698	0.837	0.951	0.596	0.337	0.7	0.52	0.152	0.2
TOP-2	0.739	0.848	0.965	0.669	0.439	0.751	0.636	0.249	0.33
TOP-3	0.760	0.85	0.968	0.699	0.49	0.778	0.636	0.322	0.4
TOP-5	0.792	0.852	0.968	0.73	0.556	0.786	0.636	0.401	0.444
TOP-10	0.831	0.853	0.968	0.751	0.588	0.788	0.636	0.472	0.488

($P<0.05$) in overall performance without any additional prompts; Moreover, not only the performance of TV-SAM method is almost as same as SAM BBOX method that relies on gold standard bbox prompts as input ($P=0.07$), but also TV-SAM even surpasses SAM BBOX method on the X-ray data (0.788 versus 0.7813).

Additionally, to further demonstrate the effectiveness of TV-SAM, we selected the three non-radiology image datasets from Fig. 2 with the best segmentation performance for comparison, such as Polyp, ISIC, and WBC.

Our TV-SAM was compared against the state-of-the-art (SOTA) results for these datasets [29, 44, 45]. These SOTA outcomes were obtained through supervised learning on the training set and evaluated on the testing set. As shown in Table 3, the performance of TV-SAM is comparable to SOTA in Polyp benchmark and even exceeds SOTA in ISIC and WBC datasets.

Furthermore, the significant performance improvement of TV-SAM over GSAM (Table 2) highlights the crucial contribution of GPT-4 in zero-shot segmentation. The rich descriptive prompts obtained from images by GPT-4 can further increase the accuracy and stability of VLM and SAM.

In some datasets like ISIC and WBC, TV-SAM outperforms the SOTA on unseen data without any manual prompts (Table 3), which further supports the paradigm shift brought about by foundation models in deep learning technology [46], emphasizing the growing importance of zero-shot and few-shot learning in practical applications.

It is crucial to emphasize that the text and visual prompts in our method are autonomously generated

and do not necessitate human intervention. This fully automated procedure operates independently of any human labeling or manual interfacing, even under zero-shot settings. Therefore, TV-SAM is more convenient and efficient than the conventional SAM methods and supervised learning methods.

For the third aspect, considering that the VLM can predict multiple bounding boxes, we further explore how to select bbox prompts to optimize SAM segmentation. As shown in Table 4, TOP-1 refers to using the highest confidence bbox predicted by VLM as the SAM prompt for segmentation, whereas TOP-k involves selecting the top k bboxes based on confidence scores and inputting them into SAM simultaneously for optimal segmentation selection.

The findings suggest while using the highest confidence bbox as the SAM prompt yields good segmentation performance, it is not the best choice.

Also, moderately increasing the number of alternative bboxes and employing SAM to operate in parallel can improve segmentation performance to some extent, especially for datasets featuring multiple target concepts or objects within a single image, which provides some guidance on how SAM selects bbox prompts.

5 Conclusion

We propose a novel multimodal medical image zero-shot segmentation algorithm, namely TV-SAM, which achieves efficient target segmentation by integrating LLM, VLM, and SAM. We implement a comprehensive evaluation on seven public datasets across eight medical imaging modalities, demonstrating the outstanding zero-shot segmentation performance of TV-SAM.

Extensive experimental results demonstrate our TV-SAM from three aspects.

Firstly, as a novel zero-shot segmentation algorithm, TV-SAM can effectively segment unseen targets across various modalities without extra training, highlighting the potential of foundational models driven prompt algorithm to solve the challenges of limited samples and multimodality in medical imaging.

Secondly, TV-SAM significantly outperforms SAM AUTO and GSAM, closely matches the performance of SAM BBOX with gold standard boxes prompts, and surpasses the SOTA on specific datasets like ISIC and WBC without additional manual prompts. This underscores the important contribution of the GPT-4 to zero-shot segmentation and shows that integrating foundational models such as LLM, VLM, and SAM can increase the ability to address complex issues.

Thirdly, by exploring the selection of bbox prompts generated by VLM, we set confidence score-based selection as a viable method for SAM prompt, noting that increasing the number of alternative boxes could modestly boost segmentation performance.

We also indicate the limitations of the current method, primarily reflected in the zero-shot segmentation performance disparity between radiology and non-radiology images.

Our analysis suggests this is not only a limitation of the TV-SAM algorithm, but also an inherent issue with all approaches based on VLM and SAM algorithms. This discrepancy is likely due to these foundational models being trained predominantly on conventional natural images, which are typically obtained through optical imaging captured by cameras. This differs fundamentally in imaging principles and modalities from radiology images, resulting in these models' relative inefficiency in processing CT and MRI images. Moreover, our study initially explores strategies to choose SAM boxes prompts, providing a general trend for selection but not specifying which alternative box prompt is the optimal choice.

Therefore, future research will focus on further

exploring how to increase TV-SAM's zero-shot performance on radiology images and investigating the best strategy for SAM bbox prompts selection to develop a more superior fully automatic zero-shot segmentation algorithm.

Acknowledgment This work was supported by grants from National Science and Technology Major Project (Nos. 2021YFF1201200, China), Chinese National Science Foundation (62372316), Sichuan Science and Technology Program (2022YFS0048), the 1·3·5 Project for Disciplines of Excellence, West China Hospital, Sichuan University (Nos. ZYYC21004), Sichuan Science and Technology Program (Nos. 2023YFG0126), and Chongqing Technology Innovation and Application Development Project (CSTB2022TIAD-KPX0067).

References

- [1] A. Kirillov *et al.*, "Segment Anything," p. arXiv:2304.02643Accessed on: April 01, 2023. doi: 10.48550/arXiv.2304.02643 Available: <https://ui.adsabs.harvard.edu/abs/2023arXiv230402643K>
- [2] W. Ji, J. Li, Q. Bi, W. Li, and L. J. a. p. a. Cheng, "Segment anything is not always perfect: An investigation of sam on different real-world applications," 2023.
- [3] L. Tang, H. Xiao, and B. J. a. p. a. Li, "Can sam segment anything? when sam meets camouflaged object detection," 2023.
- [4] R. Deng *et al.*, "Segment anything model (sam) for digital pathology: Assess zero-shot segmentation on whole slide imaging," 2023.
- [5] J. Ma, Y. He, F. Li, L. Han, C. You, and B. J. N. C. Wang, "Segment anything in medical images," vol. 15, no. 1, p. 654, 2024.
- [6] M. A. Mazurowski, H. Dong, H. Gu, J. Yang, N. Konz, and Y. J. M. I. A. Zhang, "Segment anything model for medical image analysis: an experimental study," vol. 89, p. 102918, 2023.
- [7] D. Cheng, Z. Qin, Z. Jiang, S. Zhang, Q. Lao, and K. J. a. e.-p. Li, "SAM on Medical Images: A Comprehensive Study on Three Prompt Modes," p. arXiv:2305.00035Accessed on: April 01, 2023. doi: 10.48550/arXiv.2305.00035 Available: <https://ui.adsabs.harvard.edu/abs/2023arXiv230500035K>

35C

[8] Y. Huang *et al.*, "Segment anything model for medical images?," vol. 92, p. 103061, 2024.

[9] J. Yang *et al.*, "A smart chicken farming platform for chicken behavior identification and feed residual estimation," in *2023 IEEE International Conference on Bioinformatics and Biomedicine (BIBM)*, 2023, pp. 1627-1634.

[10] J. Gao *et al.*, "Anatomically Guided Cross-Domain Repair and Screening for Ultrasound Fetal Biometry," *IEEE Journal of Biomedical and Health Informatics*, pp. 1-12, 2023.

[11] H. Song *et al.*, "Denoising of MR and CT images using cascaded multi-supervision convolutional neural networks with progressive training," (in English), *Neurocomputing*, vol. 469, pp. 354-365, Jan 16 2022.

[12] J. Gao, Q. Lao, Q. Kang, P. Liu, L. Zhang, and K. Li, "Unsupervised Cross-disease Domain Adaptation by Lesion Scale Matching," in *MICCAI 2022*, Cham, 2022, pp. 660-670: Springer Nature Switzerland.

[13] J. Gao, P. Liu, G.-D. Liu, and L. Zhang, "Robust Needle Localization and Enhancement Algorithm for Ultrasound by Deep Learning and Beam Steering Methods," (in English), *Journal of Computer Science and Technology*, vol. 36, no. 2, pp. 334-346, Apr 2021.

[14] M. Aljabri, M. AlAmir, M. AlGhamdi, M. Abdel-Mottaleb, F. J. M. t. Collado-Mesa, and applications, "Towards a better understanding of annotation tools for medical imaging: a survey," vol. 81, no. 18, pp. 25877-25911, 2022.

[15] T. Ren *et al.*, "Grounded SAM: Assembling Open-World Models for Diverse Visual Tasks," p. arXiv:2401.14159Accessed on: January 01, 2024. doi: 10.48550/arXiv.2401.14159 Available: <https://ui.adsabs.harvard.edu/abs/2024arXiv240114159R>

[16] Z. Qin, H. H. Yi, Q. Lao, and K. Li, "MEDICAL IMAGE UNDERSTANDING WITH PRETRAINED VISION LANGUAGE MODELS: A COMPREHENSIVE STUDY," in *The Eleventh International Conference on Learning Representations*, 2022.

[17] R. Schaeffer, B. Miranda, and S. J. A. i. N. I. P. S. Koyejo, "Are emergent abilities of large language models a mirage?," vol. 36, 2024.

[18] J. Wei *et al.*, "Chain-of-thought prompting elicits reasoning in large language models," vol. 35, pp. 24824-24837, 2022.

[19] Z. Xi *et al.*, "The Rise and Potential of Large Language Model Based Agents: A Survey," p. arXiv:2309.07864Accessed on: September 01, 2023. doi: 10.48550/arXiv.2309.07864 Available: <https://ui.adsabs.harvard.edu/abs/2023arXiv230907864X>

[20] A. Radford *et al.*, "Learning transferable visual models from natural language supervision," in *International conference on machine learning*, 2021, pp. 8748-8763: PMLR.

[21] Z. Liu *et al.*, "Radiology-GPT: A Large Language Model for Radiology," p. arXiv:2306.08666Accessed on: June 01, 2023. doi: 10.48550/arXiv.2306.08666 Available: <https://ui.adsabs.harvard.edu/abs/2023arXiv230608666L>

[22] L. H. Li *et al.*, "Grounded language-image pre-training," in *Proceedings of the IEEE/CVF Conference on Computer Vision and Pattern Recognition*, 2022, pp. 10965-10975.

[23] J. Cheng *et al.*, "SAM-Med2D," p. arXiv:2308.16184Accessed on: August 01, 2023. doi: 10.48550/arXiv.2308.16184 Available: <https://ui.adsabs.harvard.edu/abs/2023arXiv230816184C>

[24] H. Wang *et al.*, "SAM-Med3D," p. arXiv:2310.15161Accessed on: October 01, 2023. doi: 10.48550/arXiv.2310.15161 Available: <https://ui.adsabs.harvard.edu/abs/2023arXiv231015161W>

[25] P. Sahoo, A. K. Singh, S. Saha, V. Jain, S. Mondal, and A. J. a. p. a. Chadha, "A Systematic Survey of Prompt Engineering in Large Language Models: Techniques and Applications," 2024.

[26] Z. Shao, Z. Yu, M. Wang, and J. Yu, "Prompting large language models with answer heuristics for knowledge-based visual question answering," in *Proceedings of the IEEE/CVF Conference on*

Computer Vision and Pattern Recognition, 2023, pp. 14974-14983.

[27] Z. Yan, K. Zhang, R. Zhou, L. He, X. Li, and L. J. a. e.-p. Sun, "Multimodal ChatGPT for Medical Applications: an Experimental Study of GPT-4V," p. arXiv:2310.19061Accessed on: October 01, 2023. doi: 10.48550/arXiv.2310.19061 Available: <https://ui.adsabs.harvard.edu/abs/2023arXiv231019061Y>

[28] A. Neubeck and L. Van Gool, "Efficient non-maximum suppression," in *18th international conference on pattern recognition (ICPR'06)*, 2006, vol. 3, pp. 850-855: IEEE.

[29] D.-P. Fan *et al.*, "Planet: Parallel reverse attention network for polyp segmentation," in *International conference on medical image computing and computer-assisted intervention*, 2020, pp. 263-273: Springer.

[30] N. Codella *et al.*, "Skin lesion analysis toward melanoma detection 2018: A challenge hosted by the international skin imaging collaboration (isic)," 2019.

[31] P. Tschandl, C. Rosendahl, and H. J. S. d. Kittler, "The HAM10000 dataset, a large collection of multi-source dermatoscopic images of common pigmented skin lesions," vol. 5, no. 1, pp. 1-9, 2018.

[32] X. Zheng, Y. Wang, G. Wang, and J. J. M. Liu, "Fast and robust segmentation of white blood cell images by self-supervised learning," vol. 107, pp. 55-71, 2018.

[33] W. Al-Dhabyani, M. Gomaa, H. Khaled, and A. J. D. i. b. Fahmy, "Dataset of breast ultrasound images," vol. 28, p. 104863, 2020.

[34] H. Gong *et al.*, "Multi-task learning for thyroid nodule segmentation with thyroid region prior," in *2021 IEEE 18th international symposium on biomedical imaging (ISBI)*, 2021, pp. 257-261: IEEE.

[35] M. E. Chowdhury *et al.*, "Can AI help in screening viral and COVID-19 pneumonia?," vol. 8, pp. 132665-132676, 2020.

[36] T. Rahman *et al.*, "Exploring the effect of image enhancement techniques on COVID-19 detection using chest X-ray images," vol. 132, p. 104319, 2021.

[37] A. E. Kavur *et al.*, "CHAOS challenge-combined (CT-MR) healthy abdominal organ segmentation," *Computer Vision and Pattern Recognition*, 2023, pp. 14974-14983.

[38] M. Xiao, R. Wei, J. Yu, C. Gao, F. Yang, and L. Zhang, "CpG island definition and methylation mapping of the T2T-YAO genome," *Genomics, Proteomics & Bioinformatics*, 2024.

[39] Q. Zhang, H. Zhang, K. Zhou, and L. Zhang, "Developing a Physiological Signal-Based, Mean Threshold and Decision-Level Fusion Algorithm (PMD) for Emotion Recognition," (in English), *Tsinghua Science and Technology*, vol. 28, no. 4, pp. 673-685, 2023.

[40] L. Zhang *et al.*, "Discovering hematoma-stimulated circuits for secondary brain injury after intraventricular hemorrhage by spatial transcriptome analysis," (in English), *Front Immunol*, Original Research vol. 14, p. 1123652, 2023-February-07 2023.

[41] Y. You, L. Zhang, P. Tao, S. Liu, and L. Chen, "Spatiotemporal Transformer Neural Network for Time-Series Forecasting," *Entropy (Basel)*, vol. 24, no. 11, p. 1651, Nov 14 2022.

[42] X. Lai *et al.*, "A disease network-based deep learning approach for characterizing melanoma," *Int J Cancer*, vol. 150, no. 6, pp. 1029-1044, Mar 15 2022.

[43] Y. Xia *et al.*, "Exploring the key genes and signaling transduction pathways related to the survival time of glioblastoma multiforme patients by a novel survival analysis model," *BMC Genomics*, vol. 18, no. Suppl 1, p. 950, Jan 25 2017.

[44] Q. Xu, Z. Ma, H. Na, W. J. C. i. B. Duan, and Medicine, "DCSAU-Net: A deeper and more compact split-attention U-Net for medical image segmentation," vol. 154, p. 106626, 2023.

[45] X. Zhou, Z. Li, and T. Tong, "Medical Image Segmentation and Saliency Detection Through a Novel Color Contextual Extractor," in *International Conference on Artificial Neural Networks*, 2023, pp. 457-468: Springer.

[46] L. Zhang, S. Fan, J. Vera, and X. Lai, "A network medicine approach for identifying diagnostic and prognostic biomarkers and exploring drug repurposing in human cancer," *Comput Struct Biotechnol J*, vol. 21, pp. 34-45, 2022/11/29/ 2023.